ACS APPLIED MATERIALS & INTERFACES

Research Article

www.acsami.org

Silicon-Doped Graphene: An Effective and Metal-Free Catalyst for NO Reduction to N_2O?

Ying Chen,[†] Yue-jie Liu,[†] Hong-xia Wang,[†] Jing-xiang Zhao,*[,†] Qing-hai Cai,[†] Xuan-zhang Wang,[†] and Yi-hong Ding*[,‡]

[†]Key Laboratory of Photonic and Electronic Bandgap Materials, Ministry of Education, Key Laboratory of Design and Synthesis of Functional Materials and Green Catalysis, Colleges of Heilongjiang Province, Harbin Normal University, Harbin, 150025, China

[‡]State Key Laboratory of Theoretical and Computational Chemistry, Institute of Theoretical Chemistry, Jilin University, Changchun 130023, China

Supporting Information

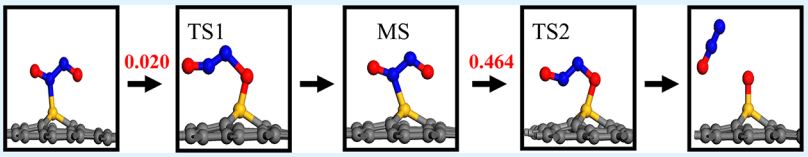

ABSTRACT: Density functional theory (DFT) calculations were performed on the NO reduction on the silicon (Si)-doped graphene. The results showed that monomeric NO dissociation is subject to a high barrier and large endothermicity and thus is unlikely to occur. In contrast, it was found that NO can easily be converted into N_2O through a dimer mechanism. In this process, a two-step mechanism was identified: (i) the coupling of two NO molecules into a $(NO)_2$ dimer, followed by (ii) the dissociation of $(NO)_2$ dimer into $N_2O + O_{ad}$. In the energetically most favorable pathway, the *trans*-$(NO)_2$ dimer was shown to be a necessary intermediate with a total energy barrier of 0.464 eV. The catalytic reactivity of Si-doped graphene to NO reduction was interpreted on the basis of the projected density of states and charge transfer.

KEYWORDS: *Si-doped graphene, NO reduction, direct dissociation mechanism, dimer mechanism, density functional theory, metal-free catalyst*

1. INTRODUCTION

The emission of pollutants has caused increasing environmental problems. The most prominent pollutants are nitrogen oxides (NO_x), which are generally produced via the fuel combustion,[1−3] and comprise about 95% NO and 5% NO_2. NO_x has been considered as a very important origin for the acid rain formation, photochemical smog, and depletion of the ozone layer.[4] Therefore, it is of utmost importance to design catalytic processes to remove or reduce NO molecules from the atmosphere. Presently, noble transition metal (such as Pt, Ag, Ru, Rh, Pd, and Au) catalysts are the most commonly used for NO reduction.[4−23] For example, the NO reduction by CO on the Pd(111) surface has been studied by Gopinath et al using molecular beam techniques with respect to temperature, NO:CO beam composition, and beam flux.[6] Chau et al.[17] have found that N_2O can be formed when NO is adsorbed on Au(111) at 300K based on their X-ray photoelectron spectroscopy (XPS) and temperature programmed desorption (TPD) studies. Theoretically, Liu et al. have shown that Ag and Ir surfaces exhibit high selectivity for NO reduction,[20−22] and Wang et al. have reported that N_2O can be easily achieved over the Au(111) surface during the NO reduction through a dimer mechanism.[23] Yet, the high costs and toxicity of the transition metal-based catalysts might greatly limit their applications for NO reduction. Thus, it is very desirable to find novel metal-free catalysts that could be effective for NO reduction.

Recently, graphene[24] has attracted tremendous attention in diverse areas due to its extraordinary properties, such as high ratio aspect, large area, and unique electronic structures.[25−35] These properties render graphene possess wide applications in gas sensing, electronic and spintronic devices, catalysts supporting, and so on.[36,37] More interestingly, the doping of graphene with guest atoms can significantly change its physical and chemical properties, thereby providing a useful means not only to manipulate the electronic, optical, and magnetic properties of graphene, but also to enhance its chemical reactivity.[38] This is of value for designing microelectronic devices, such as enhanced filed emission devices, *n*- or *p*-type semiconductors, and full cell electrodes.[38] Our interest is in the metal-free catalysts. Our previous study has suggested that the recently synthesized Si-doped graphene[39] is an effective metal-free catalyst for CO oxidation.[40] In particular, Si-doped graphene is shown to possess good stability both dynamically and thermally.[40] In terms of these excellent properties, an inspiration then rises: can Si-doped graphene be used as a catalyst for NO reduction? If can, what is the mechanism for this process? In this work, by performing density functional theory (DFT) calculations, we would address the above

Received: February 12, 2013
Accepted: June 12, 2013
Published: June 12, 2013

questions. According to our literature survey, there have been no theoretical investigations available concerning this issue. The present work would initiate more studies to develop metal-free graphene-based catalysts.

2. COMPUTIONAL DETAILS

For all the calculations in this work, we applied the spin-polarized DFT methods that are implemented in the DMol^3 code.[41,42] The generalized gradient approximation (GGA) with the Perdew-Burke-Ernzerhof (PBE) exchange-correlation functional was used,[43] in combination with the double numerical basis sets with polarization functions (DNP). During the structural optimization, no symmetry constraints were imposed. We set the convergence thresholds to be 10^{-5} Ha, 0.001 Ha/Å, and 0.005 Å, for energy, force, and displacement, respectively. Moreover, to get reliable results, we set the real-space global orbital cutoff radius to be as high as 4.6 Å and the smearing of electronic occupations to be 0.005 Ha.

For modeling a system with one carbon atom substituted by one silicon atom, we applied a hexagonal graphene supercell (4 × 4 graphene unit cells) that involves 32 atoms. To avoid the interaction of graphene and its periodic image, we set the modulus unit cell vector in the z direction to be as large as 15 Å. The 3 × 3 × 1 k points were used for calculating the Brillouin zone integration. The linear synchronous transit (LST/QST) and nudged elastic band (NEB)[44] methods were performed in order to obtain the minimum energy pathway (MEP). For each structure along the MEP, we computed the vibrational frequencies at the same level to confirm that a transition state has one and only imaginary frequency, while a minimum isomer has no imaginary frequency.

3. RESULTS AND DISCUSSION

3.1. Adsorption of NO Molecules on Si-Doped Graphene. As is well-known, the initial adsorption manner of a molecule on the catalyst surface greatly affects the subsequent surface reactions. To better understand the catalytic reactivity of Si-doped graphene toward NO molecules, the adsorptions of both NO monomer and dimer on Si-doped graphene have been calculated. The adsorption energy, E_{ads} of $(NO)_n$ (n = 1 or 2) is defined to be $E_{[(NO)n+Si\text{-doped graphene})} - nE_{(NO)} - E_{(Si\text{-doped graphene})}$, where E_X is the total energy of the X system.

For the adsorption of NO monomer on Si-doped graphene, either (i) N-atom, (ii) O-atom, or (iii) N−O bond of NO molecule could be attached to the Si or its neighboring C atom. The optimized geometries will be labeled as N_{ad}-, O_{ad}-, and $N_{ad}O_{ad}$-geometries, respectively. Though initially set to lie vertically on the surface of graphene, the NO molecule will always be tilted with respect to the surface upon optimization. Figure 1 describes the stable adsorption configurations at the Si site for both N_{ad}- and O_{ad}-forms In a titled configuration (see Figure S1 in the Supporting Information), the interaction between the highest orbital molecular orbital (HOMO) of Si-doped graphene and the $2\pi^*$ orbital of NO is symmetrically favored. The N/O atom near the Si site is associated with the largest orbital overlap. The N−O bond is elongated from 1.164 Å (in free NO) to 1.213 and 1.265 Å of N_{ad}- and O_{ad}-geometries. This is caused by the transformation of electrons (about 0.282 e) from the HOMO of Si-doped graphene to the $2\pi^*$ orbital of NO. At the same time, formation of new Si−N (1.901 Å) and Si−O (1.803 Å) bonds occurs in the two configurations. Moreover, the N_{ad}-geometry (Figure 1a, E_{ads} = −0.809 eV) is more stable than the O_{ad}-form (Figure 1b, E_{ads} = −0.192 eV). The above results are nicely consistent with previous report,[45] in which a larger supercell (7 × 7 graphene unit cells containing 98 atoms) was used. In addition, we find

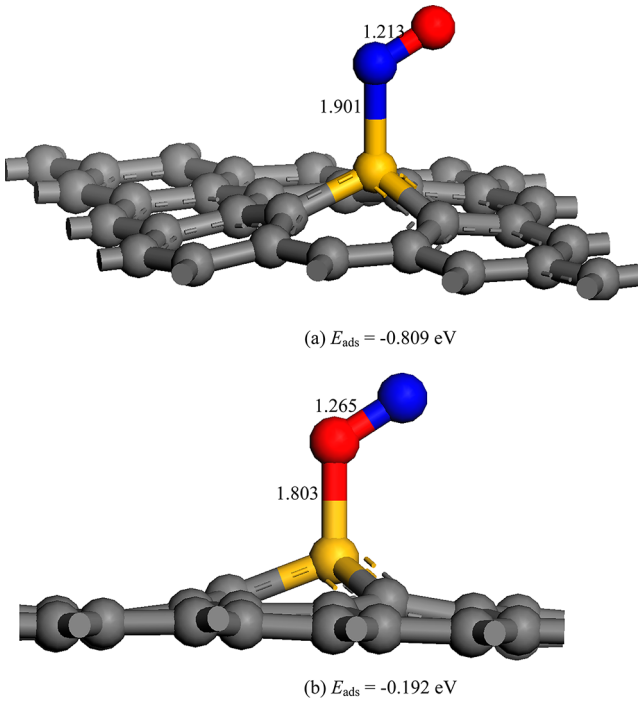

Figure 1. Optimized geometric structures of a single NO molecule on Si-doped graphene: (a) N_{ad}-geometry and (b) O_{ad}-geometry. The bond distances are in angstroms.

that the $N_{ad}O_{ad}$-geometry is unstable, which is collapsed to N_{ad}-, or O_{ad}-geometry after structural optimization.

Next, we study the adsorption of $(NO)_2$ dimer on Si-doped graphene. The gas-phase $(NO)_2$ dimer was first structurally characterized in 1970 by Dinerman and Ewing using infrared spectroscopy.[46] Recently, $(NO)_2$ dimer was also found on supported noble metal-based catalysts during NO reduction.[4−23] As shown in Figure 2, three dimers were obtained in our work. For simplicity, the three dimers are labeled as D_1 (see Figure 2a), D_2 (see Figure 2b), and D_3 (see Figure 2c), respectively. Similar to the gas phase, the NO molecules in the

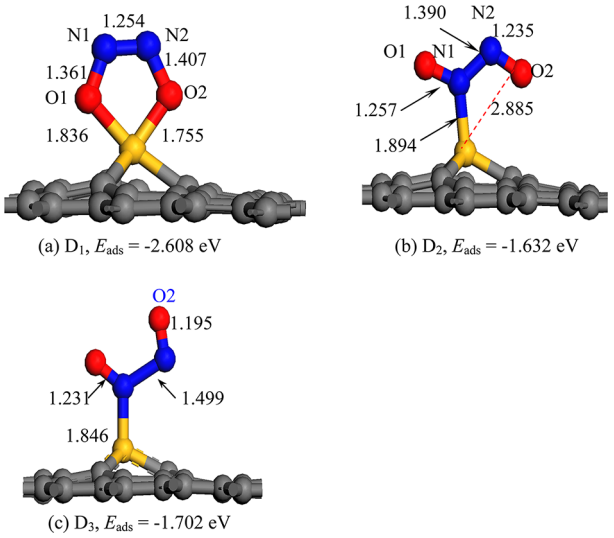

Figure 2. Optimized geometric structures and calculated adsorption energies of $(NO)_2$ dimer on Si-doped graphene: (a) D_1, (b) D_2, and (c) D_3. The bond distances are in angstroms.

dx.doi.org/10.1021/am400563g | ACS Appl. Mater. Interfaces 2013, 5, 5994−6000

three adsorbed dimers are connected to each other via a N−N bond of 1.254 (for D_1), 1.390 (for D_2), and 1.499 Å (for D_3), respectively. This is much shorter than in the gas phase $(NO)_2$ dimer (1.970 Å). Importantly, the adsorption energies of the three dimers are −2.608 (D_1), −1.632 (D_2), and −1.702 eV (D_3) with respect to the two free NO molecules, which are generally twice larger than that of the NO monomer (E_{ads} = −0.809 eV). The NO monomer adsorption on Si-doped graphene is spin-polarized, but the dimer is spin nonpolarized.

Structure D_1 (Figure 2a) is a trapezoid $O_{ad}NNO_{ad}$ species, in which the two O atoms of $(NO)_2$ dimer are adsorbed on Si atom of this doped graphene. The two formed Si−O bonds are 1.755 and 1.836 Å. Interestingly, D_1 can be easily formed when two NO monomers approach to Si-doped graphene with their O atoms being close to the Si atom (structure I), with a minimal barrier (0.056 eV, TS1 in path I of Figure 3).

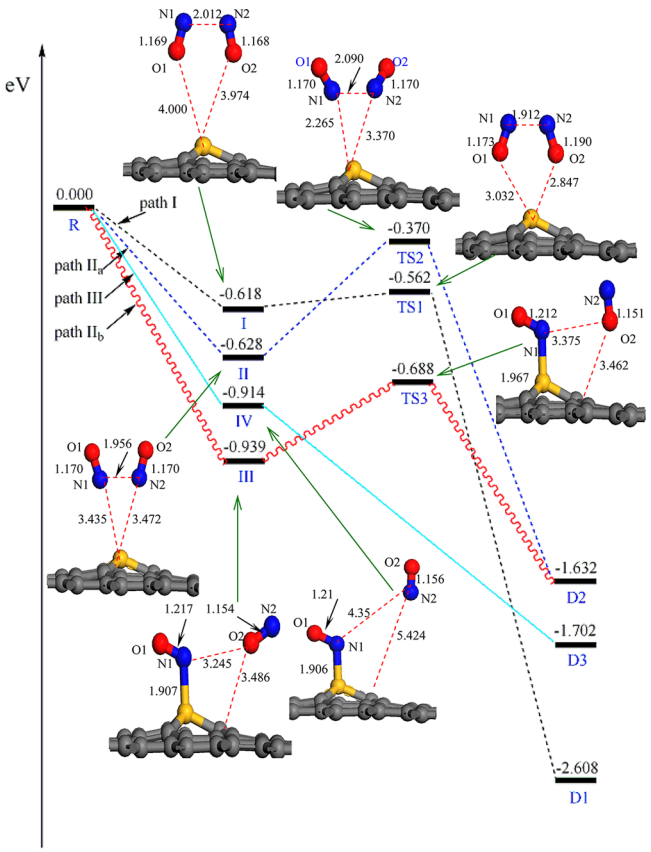

Figure 3. MEP profile with the optimized geometries of intermediates, transition states, and product for 2NO → $(NO)_2$ dimer on Si-doped graphene. Distances are in angstroms.

Structure D_2 (Figure 2b) corresponds to a *trans*-$(NO)_2$ complex, in which the distance between $(NO)_2$ dimer and Si-doped graphene is 1.894 Å. Two possible pathways were proposed to form D_2, which are denoted as path II_a and II_b. Path II_a starts from an $ON_{ad}N_{ad}O$ species (structure II), where the two NO molecules are preadsorbed on Si-doped graphene with their respective N atoms. With respect to the two free NO molecules, structure II is more stable by 0.628 eV. Once the two NO molecules are coadsorbed on Si-doped graphene, the N1 atom starts to approach the Si atom of graphene to reach TS2. The shortest distance between the adsorbed NO molecule and Si-doped graphene are shortened by 1.170 Å in this endothermic process. The energy barrier in this step is 0.258 eV. Passing over TS2, a *trans*-$(NO)_2$ dimer (i.e., D_2) is achieved over Si atom. In path II_b, two free NO molecules are adsorbed on Si-doped graphene in order, leading to the formation of structure III. It should be pointed out that structure III exhibits a triplet state, which lies below the reaction entrance by 0.939 eV. For the reaction from III to D_2, an energy barrier of 0.251 eV (for TS4) has to be overcome.

In structure D_3 (Figure 2c), which is a *cis*-$(NO)_2$ species, the lengths of N1−Si, N1−O1, and N2−O2 bonds are 1.846, 1.231, and 1.195 Å, respectively. Moreover, this dimer originates from structure IV, in which one NO molecule is first adsorbed on Si-doped graphene. Note that structure IV displays a triplet state, whose adsorption energy is calculated to be −0.914 eV with respect to the two free NO molecules. In particular, structure VI is found to easily convert into D_3 without any energy barrier, where the N2 atom of the other NO is attached to the N1 atom of the first NO (Figure 3).

It is worth emphasizing that the geometric and energetic properties of the $(NO)_2$ dimer in gas phase could not be well predicted by the pure GGA methods.[47] For instance, PBE predicts four to five times higher N−N binding energy value in $(NO)_2$ dimer than the experiment. Alternatively, the post-HF methods (CASPT2, etc) were able to provide good properties (bond lengths, angles, and binding energies).[48,49] Unfortunately, these extremely cost-expensive methods are surely not applicable to the present system. Luckily, for $(NO)_2$ dimer, some hybrid DFT methods (such as M06−2X[50]) have been shown to provide satisfactory results concerning both geometry and energetics.[51] Therefore, to verify the PBE/DNP method, we performed the M06-2X/6-31g(d) calculations on a Si-doped graphene flake cluster model ($SiC_{29}H_{14}$, see Figure S2 in the Supporting Information) using the Gaussian 09 package.[52] As successfully applied in previous studies,[53−55] we frozen the terminal hydrogen atoms that are used to saturate the dangling bonds. The obtained geometric structures of D_1, D_2, and D_3 on the basis of M06-2X calculations are shown in Figure 4. Irrespective of the difference in the applied models, the obtained geometric structures of the three dimers through the PBE/DNP and M06-2X/6-31g(d) methods generally agree well with each other. In other words, the adopted PBE/DNP method in this work can reasonably describe the behaviors of these dimers.

3.2. Mechanism of N_2O Formation. The generally accepted mechanism for NO reduction is as follows: (i) direct dissociation and (ii) and dimer mechanism. In point i, the dissociation of the first NO takes place, followed by the association of the second NO to the dissociated N-atom, forming a N_2O molecule. In point ii, the two NO molecules first undergo the coupling into a $(NO)_2$ dimer before dissociation into a N_2O molecule and an atomic O. We will discuss the above two mentioned mechanisms in more detail.

(a). Direct Dissociation Mechanism. The N_{ad}- (Figure 1a) and O_{ad}-geometries (Figure 1b) are selected as the initial states (IS). The final state (FS) is that the N and O atoms are coadsorbed on the Si-doped graphene. To achieve sufficient accuracy, 20 image structures were inserted between IS and FS. Figure 5 summarizes the corresponding MEP profile, in which the energies of Si-doped graphene and the separate NO molecule are taken as the reference energy.

As shown in Figure 5, starting from N_{ad}- and O_{ad}-geometries, the separation of N and O atoms goes through two structurally very similar late transition states ($\mathbf{TS_a}$ and $\mathbf{TS_b}$), converging to

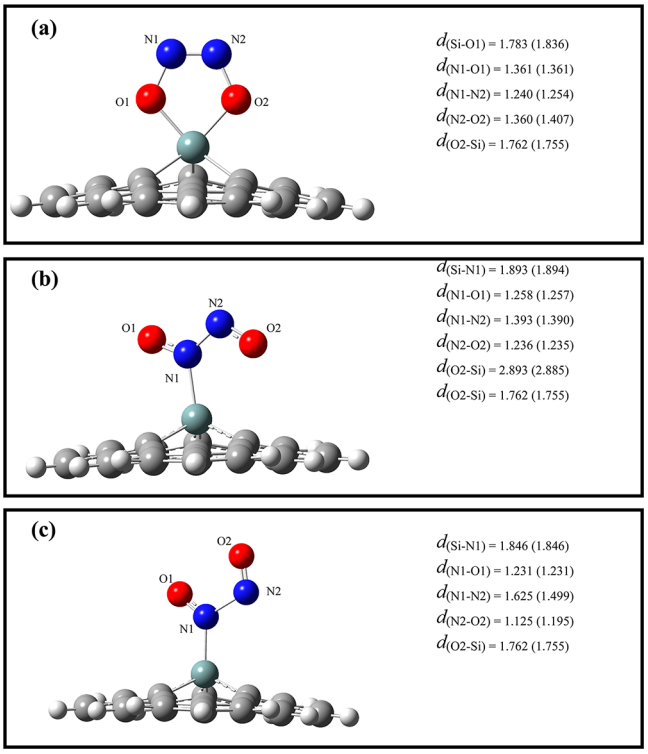

Figure 4. Optimized geometric structures of $(NO)_2$ dimer on Si-doped graphene with a cluster model at M06-2X/6-31g(d) level: (a) D_1, (b) D_2, and (c) D_3. The bond distances are in angstroms and the values in the brackets refer to the obtained bond distances using PBE/DNP method.

FS. The frequency analysis indicates that TS_a or TS_b has a single imaginary frequency (-286.28 cm^{-1} for TS_a and -285.10 cm^{-1} for TS_b), corresponding to the dissociation of N and O atoms of the adsorbed NO monomer (see the direction of red arrow in TS_a and TS_b in Figure 5). The calculated barriers for the two kinds of NO dissociation are as high as 3.909 and 3.269 eV. Moreover, the FS is more unstable than IS_a and IS_b by 1.380 and 0.763 eV. In light of the extremely high barriers and the endothermicities of the two reactions, it is expected that the ***direct*** dissociation of NO monomer on Si-doped graphene is unfavorable both kinetically and thermodynamically, suggesting that the conversion from NO into N_2O does not occur on Si-doped graphene through direct dissociation mechanism.

3.3. Dimer Mechanism for N_2O Formation. In Figure 6, we list the obtained MEP profiles along the reaction coordinate according to the dimer mechanism, as well as the corresponding minima and transition states. The electronic energies of D_1, D_2, or D_3 are taken as zero for reference.

The results indicate that structure D1 can be converted into the product (P, N_2O + O_{ads}, Figure 6a) through a transition state (TS1) with an energy barrier of 0.477 eV. For TS1, the N2−$O2_{ad}$ (1.817 Å) and the Si−$O1_{ad}$ bonds (2.433 Å) are almost ruptured. Moreover, the process of D_1 → P is exothermic by 0.750 eV. Interestingly, it is likely for structure D_1 to reduce to N_2 by breaking its two N−O bonds, leaving two oxygen atoms on the Si atom (P1). The process is exothermic by 0.318 eV and an energy barrier of 0.513 eV should be overcome. For structure D_2, as shown in Figure 6b, it is first transformed into an intermediate (MS) with a minimal energy barrier (0.020 eV, TS2). The intermediate MS is shown to be more stable by 0.556 eV than D_2. In this process of D_2 → MS, the N1−Si distance is elongated to 2.295 Å, while O2−Si distance is shortened to 1.732 Å. Crossing MS through TS3, one N_2O molecule forms. The energy barrier and the released energy for this step are 0.464 and 1.170 eV. Finally, structure D_3 can also be converted into N_2O through TS4 with an energy barrier of 0.559 eV as presented in Figure 6c.

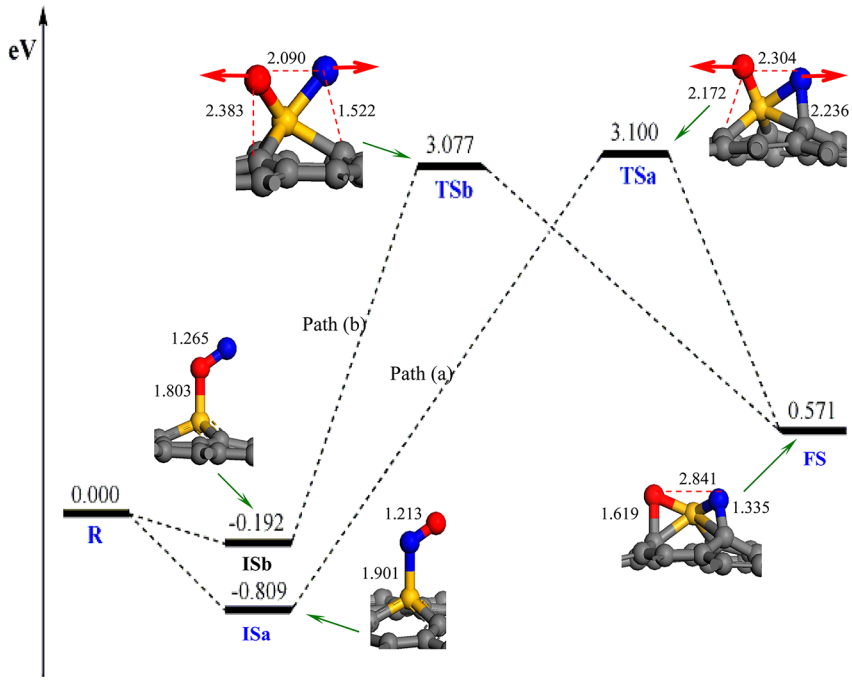

Figure 5. The MEP profile with the optimized geometries of intermediates, transition states, and product for NO direct dissociation on Si-doped graphene. Distances are in angstroms. The arrow in red denotes the direct of the vibration of the imaginary frequency.

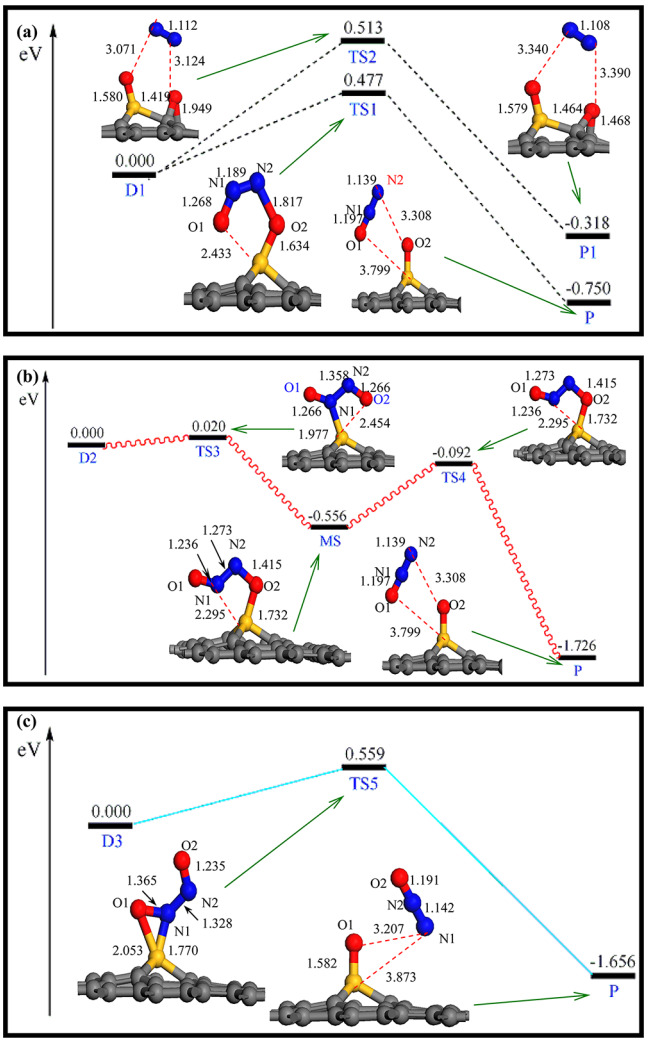

Figure 6. Schematic energy profile of 2NO → N_2O corresponding to local configurations: (a) D_1, (b) D_2, and (c) D_3 are chosen as the reactants.

In the catalysis processes, the overall barrier is generally more important than a single-step barrier. The overall barrier can be higher than that of all the single steps if one intermediate reaction is endothermic. Otherwise, the barrier of the highest single step should be the overall barrier.[56] From the calculated MEP profiles in Figure 6, we found that both the intermediate and final reaction of 2NO → N_2O + O_{ad} are exothermic. Therefore, the overall barrier should be the highest one of each path, that is, 0.477, 0.464, and 0.559 eV, respectively, for D_1, D_2, and D_3. In other words, NO molecules prefer to be reduced into N_2O via a dimer mechanism, in which the *trans*-$(NO)_2$ dimer (D_2) is a necessary intermediate. In general, a reaction with an energy barrier of less than 0.5 eV is expected to occur at room temperature. The reaction barrier of NO reduction catalyzed by Si-doped graphene is 0.464 eV, suggesting that this reaction is likely to take place rapidly at room temperature. Moreover, one can tune or enhance the catalytic activity of such graphene-based catalyst by changing the curvature of a sheet.[57,58] Compared to the traditional metal-based catalysts, such as Pt, Pd, Rh, the presently considered Si-doped graphene-based catalyst has two distinct advantages: (1) Si-doped graphene exhibits metal-free nature, which is an interesting alternative to some current industrialized chemical processes. In fact, metal-free catalysts (especially carbon-based catalysts) are friendly to environment and exhibit good thermal conductivity. They should have promise in green chemistry that requires the low emission and an efficient use of the chemical feedstock.[59] (2) Previous studies suggested that the sites of metal-based catalysts play an important role on the reduction of NO to N_2O.[21] In contrast, the Si atom of Si-doped graphene is the only catalytic active site, indicating that the selectivity of Si-doped graphene for NO reduction is considerably high.

Overall, NO reduction on Si-doped graphene intrinsically favors N_2O production by a dimer mechanism. First, the adsorption energy of the $(NO)_2$ dimer is larger than that of the NO monomer. Second, the dissociation barrier (0.464 eV) for the $(NO)_2$ → N_2O + O process is much lower than that (3.269 eV) for NO → N + O. Further examination of the electronic structures of both $(NO)_2$ and NO on Si-doped graphene could help understand the reactivity difference. Similar to the NO adsorption on transition metal surface,[22] the NO molecules bonded to the Si-doped graphene in the ionic manner to a large extent. In this case, the electrons are donated from the Si-doped graphene to adsorbates, resulting in an electrostatic attraction between the negative and positive centers. The Mulliken charge analysis showed that the accumulated net charges on NO and $(NO)_2$ are −0.282, −0.895 (for D_1), −0.493 (for D_2), and −0.378 (for D_3), respectively. This is consistent with the trend of the adsorption energy of these molecules on Si-doped graphene: $(NO)_2$ > NO. More importantly, the extra electron within $(NO)_2$ occupies the $2\pi^*$ antibonding state of the N−O bonds and the bonding state of the N−N bond, leading to the great stabilization of these dimers. Accordingly, their structural features change a lot, i.e., the N−N bond is greatly shortened in adsorbed $(NO)_2$ (1.254, 1.390, and 1.499 Å of D_1, D_2, and D_3, compared to 1.970 Å of the gas phase $(NO)_2$).

The high reactivity of Si-doped graphene toward NO monomer and $(NO)_2$ dimer can be further understood according to the projected density of states (PDOSs) (Figure 7). Bonding of $(NO)_x$ (x =1 and 2) to Si-doped graphene involves the strong hybridization between $2\pi^*$ states of $(NO)_x$ (which is unoccupied and located above the Fermi level) and 3p states of Si atom. One can notice that the maxima of the PDOS corresponds to the adsorbed $(NO)_x$ species on Si-doped graphene. When $(NO)_x$ is adsorbed on Si-doped grapheme, the $2\pi^*$ components in the PDOS spectra are partly filled and the 3p orbital of Si atom of graphene is depopulated. Thus, the catalytic activation of the adsorbed $(NO)_x$ and stretching of the N−O bond can be attributed to the partially occupied antibonding $2\pi^*$ orbital of $(NO)_x$.[47] In addition, we note that the values of PDOSs near the Fermi level of the adsorbed $(NO)_2$ dimers are generally higher than those of NO monomer, which might be a reason that Si-doped graphene exhibits higher reactivity toward $(NO)_2$ dimer than that of NO monomer. Finally, the adsorbed O atom in Si-doped graphene can be removed by CO molecule with a barrier of 0.57 eV.[40] Considering that NO_2 may be a byproduct (NO + O → NO_2) in this process, it is necessary to compare the competition between CO_2- and NO_2-formation. The results indicate that the energy barrier of NO_2-formation is 0.78 eV (see the scanned MEP profile in Figure S3 in the Supporting Information), which is slightly higher than that of CO_2 (0.57 eV).[40] Thus, CO_2 is easier to form on Si-doped graphene in the presence of CO, which is similar to some common metal-catalysts, such as Au{321}.[60]

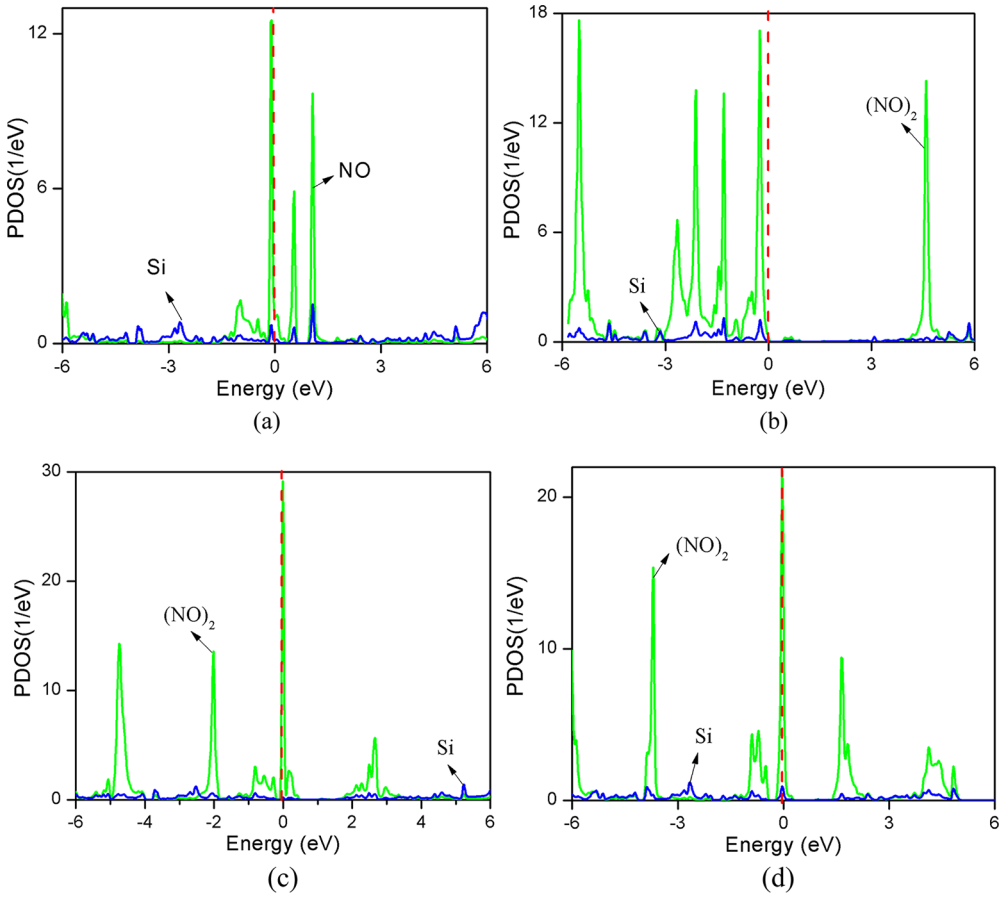

Figure 7. Calculated projected density of states (PDOS) of (a) NO monomer, (b) D_1, (c) D_2, and (d) D_3 on Si-doped graphene. The Fermi level has been set to be zero.

4. CONCLUSIONS

Through density functional theory calculations, we have investigated the reaction mechanisms of NO reduction catalyzed by Si-doped graphene through the direct dissociation and dimer mechanisms. We find that the direct dissociation mechanism is unfavorable because of the extremely high barrier and endothermicity. On the contrary, the catalytic process of NO reduction to N_2O is likely to proceed according to a dimer mechanism. On the energetically most favorable pathway, a *trans*-$(NO)_2$ complex is shown to be a necessary intermediate for the formation of N_2O. The calculated barrier for the rate-determining step along this pathway is only 0.464 eV. Furthermore, we rationalize our results by analyzing the calculated project density of states of the adsorbed monomer NO and $(NO)_2$ dimers on Si-doped graphene. The present results might be helpful to provide a guidance to develop metal-free graphene-based catalyst for NO reduction and future experimental studies are greatly desired to probe such an interesting process.

■ ASSOCIATED CONTENT

Supporting Information

Frontier orbitals of Si-doped graphene and NO molecule, cluster model of Si-doped graphene, and MEP profile of NO_2-formation on Si-doped graphene. This information is available free of charge via the Internet at http://pubs.acs.org.

■ AUTHOR INFORMATION

Corresponding Author

*Email: xjz_hmily@163.com (J.-x.Z.); yhdd@jlu.edu.cn (Y.-h.D.).

Notes

The authors declare no competing financial interest.

■ ACKNOWLEDGMENTS

This work is supported by the National Natural Science Foundation of China (No. 21203048, 21073074), the National Natural Science Foundation of Heilongjiang Province (No. B201011), and the University Key Teacher Foundation of Heilongjiang Provincial Education Department (No. 1252G030). The authors would like to show great gratitude to the reviewers for raising invaluable comments and suggestions.

■ REFERENCES

(1) Hocking, M. B. *Modern Chemical Technology and Emission Control*; Springer: Berlin, 1985.
(2) Bretschneider, B.; Kurfürst, J. *Air Pollution Control Technology*; Elsevier: Amsterdam, 1987.
(3) Cheremisinoff, P. N. *Air Pollution Control and Design for Industry*; Dekker: New York, 1993.
(4) Roy, S.; Baiker, A. *Chem. Rev.* **2009**, *109*, 4054−4091.
(5) Rosca, V.; Duca, M.; de Grott, M. T.; Koper, M. T. M. *Chem. Rev.* **2009**, *109*, 2209−2244.
(6) Hu, Y.; Griffiths, K.; Norton, P. R. *Surf. Sci.* **2009**, *603*, 1740−1750.

(7) Thirunavukkarasu, K.; Thriumoorthy, K.; Libuda, J.; Gopinath, C. *J. Phys. Chem. B* **2005**, *109*, 13272−13282.
(8) Nelin, C. J.; Bagus, P. S.; Behm, R. J.; Brundle, C. R. *Chem. Phys. Lett.* **1984**, *105*, 58−63.
(9) Behm, R. J.; Brundle, C. R. *J. Vac. Sci. Technol. A* **1984**, *2*, 1040−1041.
(10) Ludviksson, A.; Huang, C.; Jansch, H. J.; Martin, R. M. *Surf. Sci.* **1993**, *284*, 328−336.
(11) Gland, J. L.; Sexton, B. A. *Surf. Sci.* **1980**, *94*, 355−368.
(12) Salama, T. M.; Ohnishi, R.; Shido, T.; Ichikawa, M. *J. Catal.* **1996**, *162*, 169−178.
(13) Ueta, A.; Oshima, T.; Haruta, M. *Appl. Catal., B* **1997**, *12*, 81−93.
(14) Dekkers, M. A. P.; Lippits, M. J.; Nieuwenhuys, B. E. *Catal. Today* **1999**, *54*, 381−390.
(15) Debeila, M. A.; Coville, N. J.; Scurrell, M. S.; Hearne, J. R.; Witcomb, M. J. *J. Phys. Chem. B* **2004**, *108*, 18254−18260.
(16) Ilieva, L.; Pantaleo, G.; Ivanov, I.; Nedyalkova, R.; Venezia, A. M.; Andreeva, D. *Catal. Today* **2008**, *139*, 168−173.
(17) Chau, T. D.; Bocarme, T. V.; Kruse, N. *Catal. Lett.* **2004**, *98*, 85−87.
(18) Vinod, C. P.; Hansa, J. W. N.; Nieuwenhuys, B. E. *Appl. Catal., A* **2005**, *291*, 93−97.
(19) Fajin, J. L. C.; Cordeiro, M. N. D. S.; Gomes, J. R. B. *J. Phys. Chem. C* **2009**, *113*, 8864−8877.
(20) Liu, Z. P.; Hu, P. *Top. Catal.* **2004**, *28*, 71−78.
(21) Liu, Z. P; Jenkins, S. J.; King, D. A. *J. Am. Chem. Soc.* **2003**, *125*, 14660−14661.
(22) Liu, Z. P; Jenkins, S. J.; King, D. A. *J. Am. Chem. Soc.* **2004**, *126*, 7336−7340.
(23) Wang, Y.; Zhang, D.; Yu, Z.; Liu, C. *J. Phys. Chem. C* **2010**, *114*, 2711−2716.
(24) Novoselov, K. S.; Geim, A. K.; Morozov, S. V.; Jiang, D.; Zhang, Y.; Dubonos, S. V.; Grigorieva, I. V.; Firsov, A. A. *Science* **2004**, *306*, 666−669.
(25) Rao, C. N. R.; Sood, A. K.; Subrahmanyam, K. S.; Govindaraj, A. *Angew. Chem., Int. Ed.* **2009**, *48*, 7752−7777.
(26) Rao, C. N. R.; Biswas, K.; Subrahmanyam, K. S.; Govindaraj, A. *J. Mater. Chem.* **2009**, *19*, 2457−2469.
(27) Neto, A. H. C.; Guinea, F.; Peres, N. M. R.; Novoselov, K. S.; Geim, A. K. *Rev. Mod. Phys.* **2009**, *81*, 109−162.
(28) Taghioskoui, M. *Mater. Today* **2009**, *12*, 34−37.
(29) Zhu, Y.; Murali, S.; Cai, W.; Li, X.; Suk, J. W.; Potts, J. R.; Ruoff, R. S. *Adv. Mater.* **2010**, *22*, 3906−3924.
(30) Schedin, F.; Geim, A. K.; Moeozov, S. V.; Hill, E. W.; Blake, P.; Katsnelson, M. I.; Novoselov, K. S. *Nat. Mater.* **2007**, *6*, 652−655.
(31) Barbolina, I. I.; Novoselov, K. S.; Morozov, S. V.; Dubonos, S. V.; Missous, M.; Volkov, A. O.; Christian, D. A.; Grigorieva, I. V.; Geim, A. K. *Appl. Phys. Lett.* **2006**, *88*, 013901.
(32) Allen, M. J.; Tung, V. C.; Kaner, R. B. *Chem. Rev.* **2010**, *110*, 132−45.
(33) Loh, K. P.; Bao, Q.; Ang, P. K.; Yang, J. *J. Mater. Chem.* **2010**, *20*, 2277−2289.
(34) Terronesa, M.; Botello-Méndez, A. R.; Campos-Delgado, J.; López-Urías, F.; Vega-Cantú, Y. I.; Rodríguez-Macías, F. J.; Elías, A. L.; Muñoz-Sandoval, E.; Cano-Márquez, A. G.; Charlier, J.-C.; Terrones, H. *Nanotoday* **2010**, *5*, 351−372.
(35) Abergel, D. S. L.; Apalkov, V.; Berashevich, J.; Ziegler, K.; Chakraborty, T. *Adv. Phys.* **2010**, *59*, 261−482.
(36) Biró, L. P.; Nemes-Incze, P.; Lambin, P. *Nanoscale* **2012**, *4*, 1824−39.
(37) Guo, S. J.; Dong, S. *J. Chem. Soc. Rev.* **2011**, *40*, 2644−2672.
(38) Terrones, H.; Lv, R. T.; Terrones, M.; Dresselhaus, M. S. *Rep. Prog. Phys.* **2012**, *75*, 062501.
(39) Chishlom, M. F.; Duscher, G.; Windl, W. *Nano Lett.* **2012**, *12*, 4651−4655.
(40) Zhao, J. X.; Chen, Y.; Fu, H. G.. *Theor. Chem. Acc.* **2012**, *131*, 1242.
(41) Delley, B. *J. Chem. Phys.* **1990**, *92*, 508−517.
(42) Delley, B. *J. Chem. Phys.* **2000**, *113*, 7756−7764.
(43) Perdew, J. P.; Burke, K.; Ernzerhof, M. *Phys. Rev. Lett.* **1996**, *77*, 3865−3868.
(44) Henkelman, G.; Jonsson, H. *J. Chem. Phys.* **2000**, *113*, 9978−9985.
(45) Chen, Y.; Gao, B.; Zhao, J. X.; Cai, Q. H.; Fu, H. G. *J. Mol. Mod.* **2012**, *18*, 2043−2054.
(46) Dinerman, C. E.; Ewing, G. E. *J. Chem. Phys.* **1970**, *53*, 626−631.
(47) Mazheika, A.; Bredow, T.; Ivashkevich, O. A.; Matulis, V. E. *J. Phys. Chem. C* **2012**, *116*, 25262−25273.
(48) SayóS, R.; Valero, R.; Anglada, J. M.; González, J. *J. Chem. Phys.* **2000**, *112*, 6608−6624.
(49) Glendening, E. D.; Halpern, A. M. *J. Chem. Phys.* **2007**, *127* (164307), 1−11.
(50) Zhao, Y.; Truhlar, D. G. *Theor. Chem. Acc.* **2008**, *120*, 215−241.
(51) Cramer, C. J.; Truhlar, D. G. *Phys. Chem. Chem. Phys.* **2009**, *11*, 10757−10816.
(52) Frisch, M. J. et al. *Gaussian 09*, revision A.01; Gaussian, Inc.: Wallingford, CT, 2009.
(53) Nunzi, F.; Mercuri, F.; Sgamellotti, A.; Re, N. *J. Phys. Chem. B* **2002**, *106*, 10622.
(54) Nunzi, F.; Mercuri, F.; Angelis, F. D.; Sgamellotti, A.; Re, N.; Giannozzi, P. *J. Phys. Chem. B* **2004**, *108*, 5234.
(55) Zhao, J. X.; Xiao, B.; Ding, Y. H. *J. Phys. Chem. C* **2009**, *113*, 16736−16740.
(56) Song, E. H.; Wen, Z.; Jiang, Q. *J. Phys. Chem. C* **2011**, *115*, 3678−3683.
(57) Boukhvalov, D. W.; Katsnelson, M. I. *J. Phys. Chem. C* **2009**, *113*, 14176−14178.
(58) Lu, Y. H.; Zhou, M.; Zhang, C.; Feng, Y. P. *J. Phys. Chem. C* **2009**, *113*, 20156−20160.
(59) Su, D. S.; Zhang, J.; Frank, B.; Thomas, A.; Wang, X.; Paraknowitsch, J.; Schlögl, R. *Chem. Sus. Chem.* **2010**, *3*, 169−180.
(60) Fajín, J. L. C.; Cordeiro, M. N. D. S.; Gomes, J. R. B. *J. Catal.* **2012**, *289*, 11−20.